5 Process-based investigations and monitoring of deep-seated landslides

C. Zangerl, C. Prager, W. Chwatal, S. Mertl, D. Renk, B. Schneider-Muntau, H. Kirschner, R. Brandner, E. Brückl, W. Fellin, E. Tentschert, S. Eder, G. Poscher, H. Schönlaub

5.1 Introduction

Through the consolidation of alpine settlement areas there have been an increasing number of incidents in recent years related to the activity of landslides in Northern Tyrol (Austria). This has led to humans, buildings, and communication and transportation routes being increasingly threatened. In 1999 a rockfall event in Huben (Ötztal, Austria) destroyed a wood mill and cut the main power supply for the inner Ötztal. In the same year increased deformation rates at the Eiblschrofen (Schwaz, Austria) induced reoccurring rockfall events. In early summer 2003, parts of the deep-seated Steinlehnen rockslide system (Gries i. Sellrain, Austria) were reactivated, causing an acceleration of a sliding slab (Henzinger 2005). Secondary events in the form of increased rockfall activity were the direct consequence of these slope movements and demanded temporary evacuations and roadblocks as immediate measure. In order to protect the road and settlement area permanently a safety dam was built. After the floods in Tyrol in August 2005, parts of the complex Zintlwald landslide system (Strengen, Austria) accelerated. This was triggered on the one hand by increased water infiltration of the slope and on the other hand by intense fluvial erosion of the slope foot. As a consequence important supra-regional infrastructure such as sections of the Arlberg national road were destroyed. In addition, the possibility was given that a rapid landslide could dam the river Rosanna. Considering that a collapse of this dam would entail a sudden flood event downstream, a monitoring and warning system has been installed.

This case study showed that slowly moving slopes can develop into rapid landslides with a high power of destruction. More often they can lead to differential block movements causing damage to the infrastructure on the surface and below the ground. For instance, long and wide cracks were discovered on buildings situated on the deep-seated Niedergallmigg-Matekopf landslide (Fließ, Austria, Kirschner and Gillarduzzi 2005).

E. Veulliet et al. (eds.), *Sustainable Natural Hazard Management in Alpine Environments*,
DOI 10.1007/978-3-642-03229-5_5, © Springer-Verlag Berlin Heidelberg 2009

Landslides that occur close to reservoirs possess a generally high risk potential and thus require detailed investigation and permanent monitoring. These landslides offer ideal conditions for the comprehensive study of the underlying slope mechanisms and processes, because they provide long-term deformation measurements, well documented in-situ investigations e.g. boreholes, investigation adits and geophysical surveys (e.g. Leobacher and Liegler 1998, Tentschert 1998, Brückl et al. 2004, Watson et al. 2004, Zangerl et al. 2007).
This paper focuses on basic mechanical processes, temporal activity distributions, applied geophysical investigations and monitoring methods of deep-seated landslides in fractured rock masses.

5.2 Landslide classifications

A simple and clear definition for the term "landslides" was proposed by Cruden (1991) and taken on by the International Geotechnical Society, UNESCO Working Party on World Landslide Inventory and represents the beginning of an international harmonising of the mass movement nomenclature: "*Landslide is a movement of a mass of rock, earth or debris down a slope"*. This definition includes debris flows but not ground subsidence or snow avalanches.
However literature offers a large number of different classification schemes for landslides. Due to the complexity and ambiguity of different terms, which is particularly the case in German-speaking countries, this paper refers to the practical and useful classification of Varnes (1978) and Cruden and Varnes (1996). In principal, these categorisations are based on the type of movement and type of material.
According to this, landslide movement types are termed as falls, topples, slides, spreads and flows, whereas complex landslide systems may be classified by a combination of different terms. In regard to the type of material it is possible to differentiate between rock and soil. For the further description of landslides Varnes' (1978) classification also includes a subdivision into different classes of acceleration, ranging from "extremely slow" for movement rates of under 16 mm/a to "extremely rapid" when there is acceleration of over 5 m/s.

5.3 Temporal distribution of dated landslides in the East Alpine region

Landslides are characterised by complex combinations of geological, hydrogeological, rock or soil mechanical and climatic processes. In order to understand potential causes, trigger mechanisms and the temporal distribution of deep-seated landslides geochronological data of fossil and active case studies were compiled. Age dating of landslides in the Alps was previously based on relative criteria such as geomorphological and lithostratigraphical field evidences. Consequently it was assumed that flucio-glacial erosion and glacier withdrawals triggered numerous prominent landslides in the Late-Glacial and early Post-Glacial (e.g. Abele 1974). But already early attempts of age dating, by means of pollen analysis of lake sediments that are genetically linked with landslides, indicated that some landslides took place in the Holocene (e.g. Sarnthein 1940). This was confirmed by first radiometric C-14 dating of Alpine landslides, e. g. the rocklslides at Molveno (Trentino, Italy), Köfels and Hochmais (both Tyrol, Austria), which yielded clearly Holocene ages for the slope failures (Marchesoni 1958, Heuberger 1966, Schmidegg 1966). Further dating showed that also several other deep-seated rockslides, e.g. in the Tschirgant (Tyrol; Patzelt and Poscher 1993) and Eibsee region (Bavaria; Jerz and Poschinger 1995) took place in the middle Holocene and not as previously believed in the Late-Glacial.

For the dating of Quaternary sediments and prehistoric landslide deposits there are a number of different radiometric analysis methods available (e.g. Geyh and Schleicher 1990, Lang et al. 1999). In the Eastern Alps, the majority of landslides were dated with the classic radiocarbon method, using organic remnants that are a) present in sediments buried by the rockslide (maximum age of the event), b) trapped within the rockslide debris (proxy for the event), and/or c) that were deposited in rockslide-dammed backwater deposits or lakes situated atop the rockslide mass (minimum age of the event). In recent years, new absolute age dating methods have been developed and increasingly applied. Among these are surfaces exposure dating using in-situ-produced cosmogenic radionuclides, applied e. g. at sliding planes and accumulated rockslide boulders of the Köfels landslide (Tyrol; Ivy-Ochs et al. 1998), optically stimulated luminescence (OSL) methods for dating landslide deposits and associated backwater sediments as well as U-/Th dating methods. At the prominent Fernpass rockslide, which is one of the largest landslide of the Alps, the field situation enabled the application of three individual dating methods on samples from geologically different localities (Prager et al. 2008a, Ostermann et al. 2007), which are a)

C-14 dating of organic material accumulated in rockslide dammed backwater deposits, b) Cl-36 exposure dating of sliding planes at the scarp (and accumulated rockslide boulders), and c) Th-230/U-234 disequilibrium dating of post-failure aragonite cements that precipitated in the pore-cavities of the landslide deposits. All dating data coincide well and indicate that the Fernpass rockslide took place in the middle Holocene at about 4200-4100 yrs.

Based on this, and in order to evaluate the spatial and temporal distribution of mass movements in Tyrol and its surrounding areas, a GIS linked geodatabase was set up. For the first time all available radiometric data of lateglacial and Holocene landslides in the East Alpine region were compiled (Fig. 5.1). Analyses of these data indicate that both rock slope failures (e. g. rockslides, rockfalls) and debris flows occurred rather continuously distributed in the Late-Glacial and Holocene. However, it is noticeable that there are two temporal clusters of increased landslide activities: a) in the early Holocene between 10500-9400 BP, comprising the large rockslides of Köfels, Kandertal and Flims, and b) in the middle Holocene between 4200-3000 BP, when several of the largest landslides in the Eastern Alps took place (e.g. Eibsee, Fernpass, Tschirgant, Haiming, Pletzachkogel).

Furthermore, the compiled age data show that several slopes were repeatedly reactivated in the Holocene. Multiple failure events in the Alpine region were, amongst others, documented in the following areas:

- Fernpass rockslide (Tyrol): a main large-scale failure event in the middle Holocene, a laterally adjacent secondary rockslide and the initial stage of a rockslide were observed (Prager et al. 2007);
- Tschirgant massif (Upper Inntal, Tyrol): two distinct scarp regions featuring at least five different failure events in the middle Holocene (Patzelt 2004);
- Köfels (Oetztal, Tyrol): one major rockslide in the early Holocene and at least one larger secondary event (Ivy-Ochs et al. 1998, Hermanns et al. 2006);
- Tumpen (Oetztal, Tyrol): several failure events, two of which dated roughly around the middle Holocene (Poscher & Patzelt 2000);
- Pletzachkogel (Lower Inntal, Tyrol): at least three temporally differing rockslide events in the Late-Glacial and middle Holocene, as well as smaller rockfall events in the 20th century (Patzelt 2004);
- Multiple reactivations or accelerations of pre-existing landslides in time intervals of a few thousand years were observed in Gepatsch-Hochmais (Kaunertal, Tyrol; Schmidegg 1966), Heinzenberg (Switzerland, Weidner 2000) and La Clapière (France, Cappa et al. 2004);

- Several cases of recent landslides, such as the in Val Pola (1987, Italy) and Randa (1991, Switzerland) have shown that failure was structurally controlled and that there were precursory events in (pre-historic times (Azzoni et al. 1992, Sartori et al. 2003).

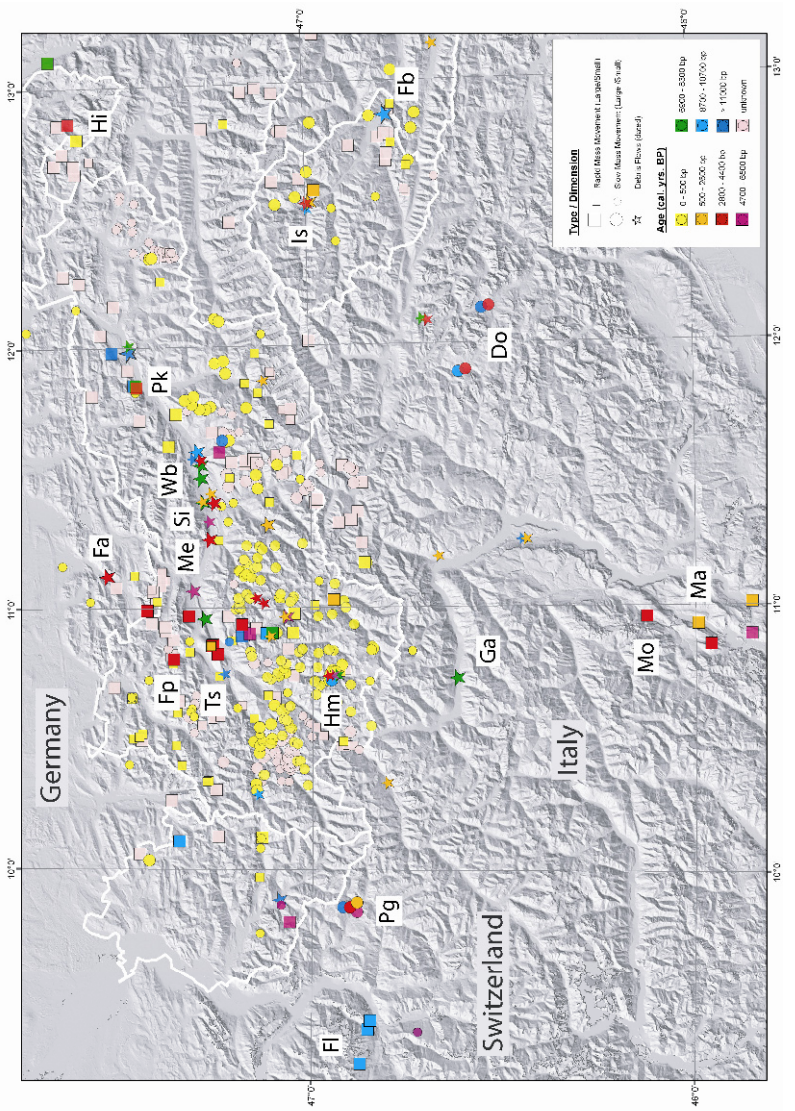

Fig. 5.1 Spatial and temporal distribution of mass movements in the Tyrol (Austria) and its surrounding areas (Prager et al. 2008b). Beyond Tyrol only dated fossil landslides are shown. *Do*: Dolomites rock slope failures, *Fa:* Farchant debris flow, *Fb*: Frauenbach debris flows, *Fl*: Flims rockslide, *Fp*: Fernpass rockslide, *Ga*: Gadria river, *Hi*: Hintersee rockslide, *Hm*: Hochmais rockslide, *Is*: Isel river, *Ma*: Marocche di Dro, *Mo*: Molveno rockslide, *Me*: Melach river, *Pg*: Prättigau rock slope failures, *Pk*: Pletzachkogel rockslides, *Si*: Sill river, *Ts*: Tschirgant rockslide, *Wb*: Weißenbach river

However, not only rock slope failures but also dated debris flows show fluctuating activities in the Holocene. Periods of increased debris accumulation rates were established for the Tyrolean Inn valley and its main tributaries, occurring at about 9400, between 7500-6000 and at around 3500 C-14 years (Patzelt 1987), and were probably climatically controlled by the amount of water in the catchment areas. These periods partially correlate temporally with glaciers advances in the Austrian Central Alps (Patzelt 1977) as well as with several other large landslides in the Eastern Alps (Fig. 5.2).

Hence, these data suggest that the stability conditions of numerous fossil landslides were affected by the climatically controlled water pressure distribution in the slopes. Similar phases of increased slope instabilities were previously detected in the Swiss and North Italian Alps (Fig. 5.2) and generally attributed to climate changes (Raetzo-Brülhart 1997, Dapples et al. 2003, Soldati et al. 2004).

The principal cause for Alpine landslides may be ascribed to glacier retreats, but this was not necessarily the direct trigger. In fact, the majority of slopes remained in a "stable" position for several thousands of years, after ice-withdrawal, before complete collapse set in. Detailed field studies and compiled geological data indicate that deep-seated slope deformations may generally be attributed to the propagation and coalescence of brittle discontinuities. Progressive failure is induced by complex interactions of different time-dependent processes such as a) stress redistributions due to glacial loading and unloading, b) subcritical crack growth, c) seismic activity and d) climatically controlled pore pressure changes (Prager et al. 2008b).

As a result, the analyses of the compiled data set shows that a) periods of significantly increased mass movement activity are distinguishable (Fig. 5.2), b) spatial accumulations of slope instabilities occur (Fig. 5.1) and c) predisposed areas were repeatedly (re)activated for mass movements and even posses high risk potential of future events. Consequently, well documented case studies indicate that the pre-failure mechanisms are of essential importance for the early detection of endangered settlement and economic areas.

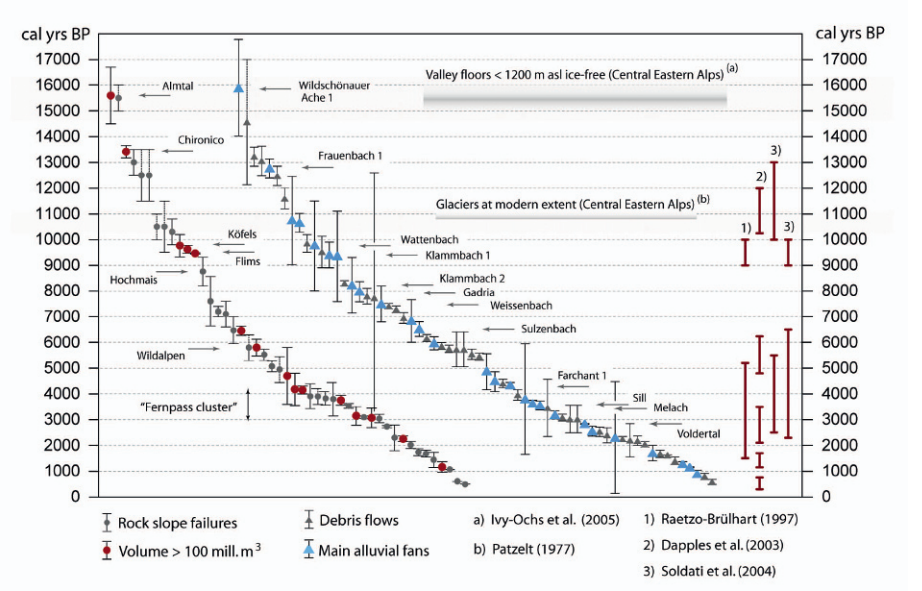

Fig. 5.2 Temporal distribution of fossil mass movements in Tyrol and the surrounding region (Prager et al. 2008b). Vertical axis = calibrated years before present (BP = before present), horizontal axis = dimensionless sequence of dated events

5.4 Basic principles of deformation and failure processes of landslides

For the estimation of the hazard potential of landslides it is decisive to understand the failure mechanisms, the deformation behaviours and the slope kinematics. Thus, for example, any sound forecast of slope instabilities is fundamentally affected by whether a translational or rotational slide prevails, or whether toppling or falling processes or complex combinations of both dominate the slope deformation. Only combined analyses of geological, hydrological, geomorphological, geodetical, geophysical and other exploratory data (e.g. boreholes and investigation adits) enables the development of a comprehensive model, which is able to represent the natural system characteristics as close as possible.

5.4.1 Fracture mechanical processes

The steeply inclined scarps on rockfall locations indicate that slope failures are induced by fracture mechanical processes such as fracture growth of new and coalescence of already existing fractures. Einstein et al. (1983) and Eberhardt et al. (2004) assume, that fully persistent discontinuities seldom occur in nature, and much rather that slope failures are induced by interactions of existing discontinuities and fracture propagation. In general a jointed rock mass consists of intact rock blocks (including microcracks and micropores), which are bound by discontinuities such as bedding planes, joints and fault zones. Intact rock bridges between these discontinuities increase the strength of a rock mass. This means that the stability of rock slopes is determined by the orientation, density and size of fractures in a rock mass (Einstein 1993).

Fracture propagation strongly depends on the existing stress field as well on the fracture geometry and network (Einstein and Stephansson 2000). In regard to the development of fractures there are three different basic fracture modes: mode I = opening, mode II = sliding, in-plane shear and mode III = scissoring, anti-plane shear. Naturally complex combinations of these three modes are likely to occur. Classical fracture mechanics postulates that in a linear, elastically solid body fracture propagation takes place with acoustic velocity of the medium when a critical stress intensity factor (K_{IC} for mode I, K_{IIC} for mode II) is reached in the crack tip. In the case of a stress intensity factor K_I (or K_{II}) below the critical stress intensity factor the crack remains stable.

However, there are physical-chemical processes in fractures that enable slow crack propagation even below this K_{IC}-threshold, referred to as sub-critical crack growth (Fig. 5.3; Atkinson 1984). Due to the complex interactions of pore pressure, stress corrosion, dissolution, diffusion, ion exchange and microplasticity it is very difficult or nearly impossible to estimate the time factor for this mechanism. For example, the process of stress corrosion, which is characterised by weakening of crystal bonds through chemical fluid activities (e.g. water) in the crack tip, leads to slow crack propagation. The application of this fracture mechanical model on unstable slopes would, however, mean that over a longer time period the fracture density and persistence continuously increase. In the long term this leads to a continuous decrease in the slope stability and to a failure event when the strength threshold is exceeded.

Besides the sub-critical and critical crack growth, also temperature effects must be considered when dealing with rather shallow seated rockfall events. In-situ measurements at the rockfall Val d'Infern (Graubünden, Switzerland) show, that temperature induced stress changes affect the rock

mass to depths of about 10 m. These cyclical loading conditions lead to progressive fracture displacements and thus reduce the long-term stability (Krähenbühel 2004). Furthermore the stability of Alpine rock flanks may also be influenced by permafrost conditions, depending on the exposition, inclination and elevation of the slope.

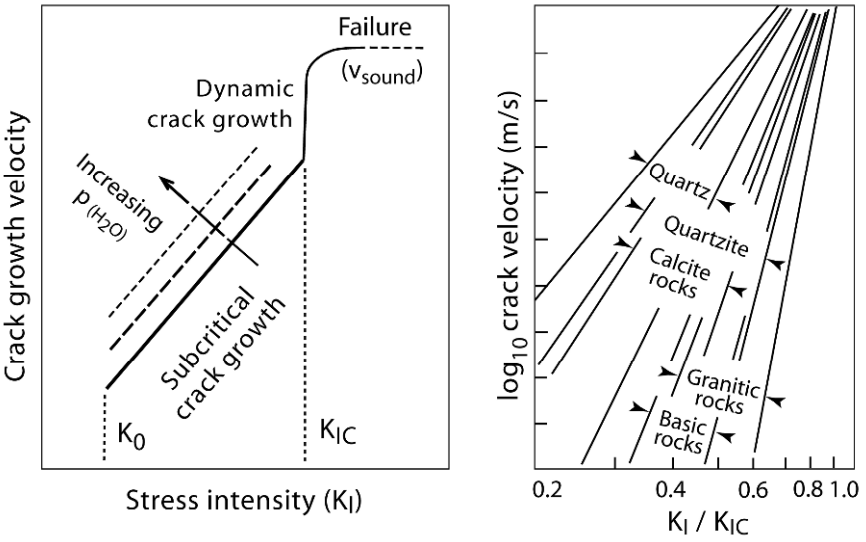

Fig. 5.3 Schematic illustrations showing (on the left) crack growth velocity versus stress intensity factor (K_I) for Mode I loading: sub-critical crack growth starts when driving forces exceed a threshold K_0. Approaching to a critical level K_{IC}, cracks propagate dynamically to near the velocity of sound in the rocks. Note that increasing pore pressures $p_{(H20)}$ may significantly accelerate crack propagation velocities. On the right, variations of sub-critical tensile crack growth in different rock types are shown (log/log plot; arrows indicate range of experimentally obtained data; K_{IC}=fracture toughness, K_o=stress corrosion limit; modified after Atkinson 1984, 1987)

Given the extremely complex interactions of the physical and chemical processes discussed above, the time-dependent reduction of rock mass strength is difficult to forecast without any deformation monitoring data. So far only a few fracture mechanical based stability approaches are published. For example, a time-dependent cohesion loss model derived by Kemeny (2003) suggests that after a phase of progressive strength reduction slope failure occurs very rapidly. This and some case studies show that long lasting deformation phases preceded the failure event. For example, pre-failure deformation measurements in the region of a rockfall near

the Jungfraujoch (Switzerland) proved that the actual event was preceded by rock deformation phases of at least one year (Keusen 1998). A high resolution monitoring device based on extensometers was installed 85 days before the failure event. Whereas during the first 2 months after installation a relatively linear displacement trend was measured (total displacement of 4 mm), the slope started to accelerate 2.5 weeks before failure and finally collapsed after another 10 mm of displacement. Also geodetic measurements at the rockfall Val d'Infern, which were performed between 1995 and 2006, showed increasing slope velocities before it collapsed (Krähenbühl 2006). Based on such acceleration patterns, the time of slope failure can be determined by analyses of inverse slope velocities versus time (Voight 1988).

5.4.2 Sliding processes

If a fully persistent sliding zone is formed through fracture mechanical processes, then further slope deformation is essentially determined by sliding processes resulting from material creep and/or shear slip in these zones. The sliding mass itself is mostly characterised by relative little internal deformation. Whether a fully persistent sliding zone can exist within a slowly creeping, deep-seated landslide has often been debated controversially, but is highly relevant for stability analysis. In some cases detailed field investigations show that surface deformation is obviously the result of flexural or block toppling mechanisms without any indications of a continuous sliding zone (Zischinsky 1969, Amann 2006). However, in many cases the slope kinematics is clearly characterised by sliding mechanisms. This is confirmed by several field observations and inclinometer measurements on landslides showing a) extensive sliding planes in the scarp area, b) a discrete offset between sliding masses and the stable bedrock unit, c) lateral exposures of sliding zones and d) kakirites (i.e. uncemented breccias and gouges) acting as active sliding zones. Also data obtained from boreholes and investigation adits in Switzerland (Noverraz 1996) show that the major deformation of deep-seated mass movements generally occurs along discrete sliding zones (Fig. 5.4).

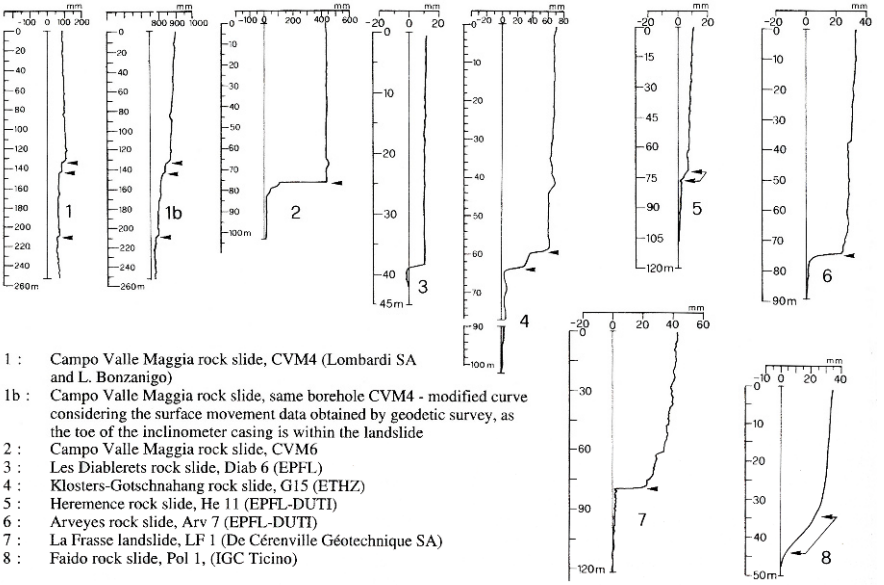

Fig. 5.4 Inclinometer data of seven deep-seated landslides in Switzerland showing major displacement along discrete sliding zones (Noverraz 1996)

Similar results were obtained from several rockslides in the Tyrolean Alps (e.g. Gepatsch/Kaunertal, Gries/Sellraintal), where one or more sliding zones control slope deformation and kinematics (Zangerl et al. 2007). Exploration adits, borehole data and field surveys show that these sliding zones can extend to thicknesses of several metres and consist of slope failure induced kakirites. These sliding zone kakirites are characterized by intensively fractured, fragmentised and triturated rocks which are generally difficult to distinguish from tectonically formed fault breccias and gouges. Several field studies show that already existing tectonic fault zones are often reactivated as sliding zones of landslides (Fig. 5.5). Conclusively it was found that many of the investigated landslides are in fact “slides” which are characterised by slipping along discrete shear planes and/or creeping within one or several sliding zones. In this case “creeping” is defined as a continuous material deformation under constant stress state (e.g. Hudson and Harrison 1997).

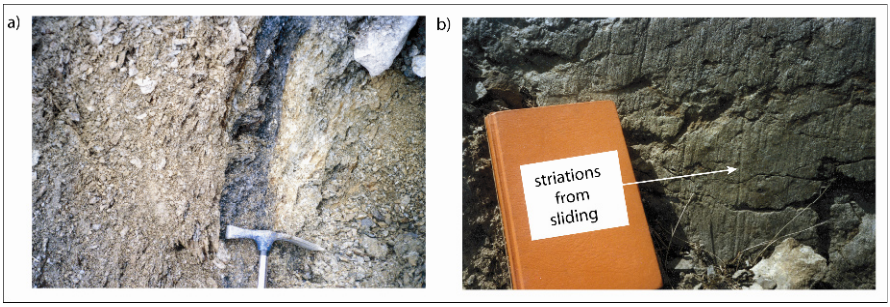

Fig. 5.5 a) Tectonically formed kakirite of a brittle fault zone acting as a mass movement sliding zone, b) slope failure induced slickenside striations (landslide system Steinlehnen, Tyrol; location see Fig. 5.13)

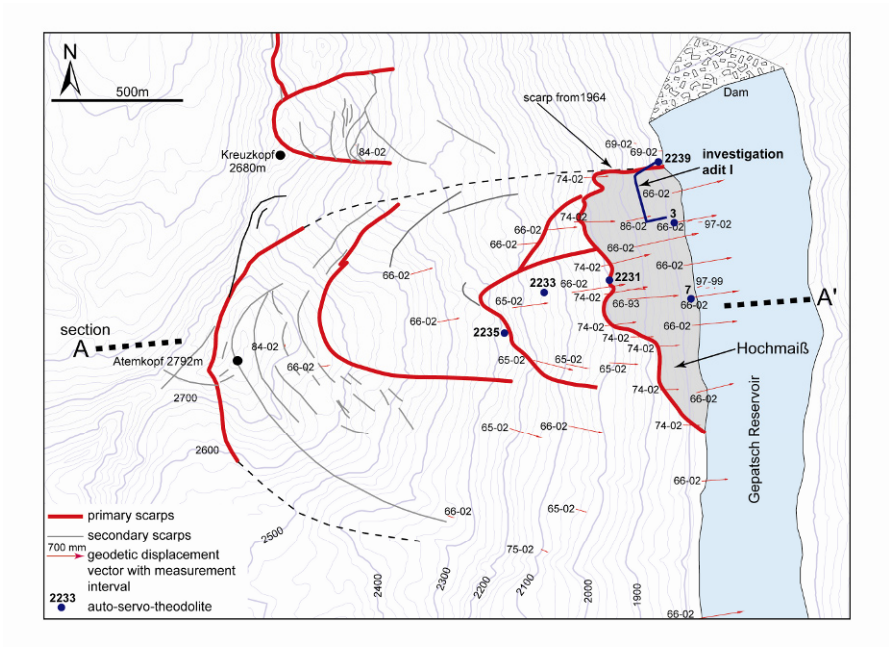

Fig. 5.6 Map of the Hochmais-Atemkopf rockslide (Kaunertal, Tyrol) and its monitoring system showing: a) primary and secondary scarps of different sliding slabs (red lines; grey coloured: Hochmais slab), b) episodic triangulation points (red arrows), c) automatic total station measurements (blue points), d) investigation adit that passes from the stable bedrock into the Hochmais slab (see Fig. 5.7)

In the Kaunertal, the active sliding slab Hochmais has slid over glacial till and talus material and continued to move towards the valley bottom (Fig. 5.6). Exploration adits and boreholes document that the sliding zone did

not form directly between the sliding mass and its soil substrate beneath, but much rather a 4 to 5 m thick sliding zone developed within the glacial till itself (Fig. 5.7). In the exploration adit, which intersects the active movement zone, permanent measurements are taken with a wire extensometer in order to measure the horizontal displacement vector. In addition vertical displacements have been measured by means of episodic levelling. Based on a linear regression analysis of both data sets the E-W orientated displacement vector at the base of the sliding mass dips about 32° to the East (Fig. 5.8). Comparisons with levelling und triangulation measurements on the surface of the sliding mass show similar slope velocities and dip angles as observed in the sliding zone. Thus, the Hochmais rockslide represents a slide along a several meter thick distinct deformation zone, whereby the internal deformation of the sliding mass is comparatively small.

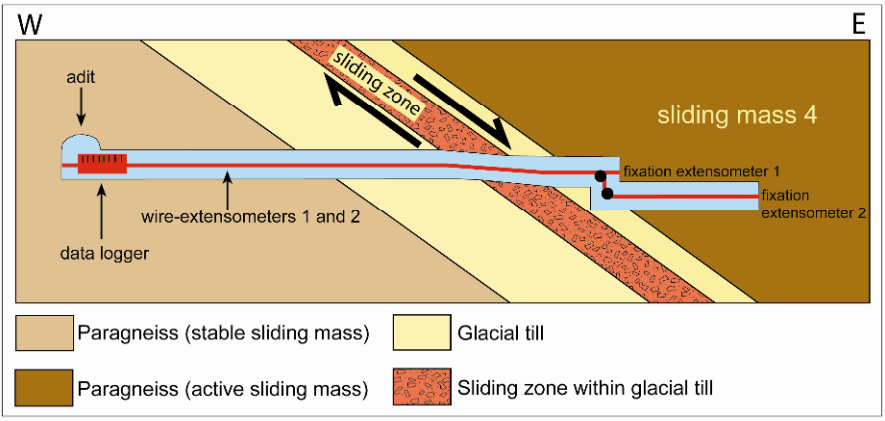

Fig. 5.7 Schematic illustration of the exploration adit which intersects both the stable bedrock and the active sliding slab Hochmais (Kaunertal, Tyrol). Along this adit interval, a wire extensometer device, a water level gauge and levelling points were installed

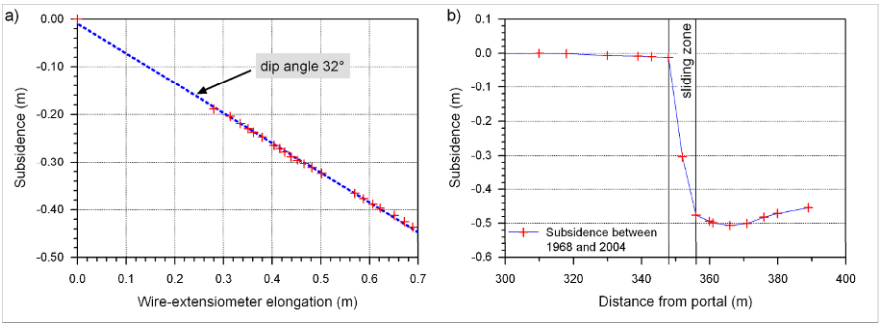

Fig. 5.8 a) Linear regression between levelling and wire extensometer measurements and the resulting dip angle of the displacement vector at the base of the active sliding slab Hochmais, b) calculated subsidence between both levelling measurements in 1968 and 2004 around the movement zone in the exploration adit. The levelling measurements in the region of the sliding zone showed subsidence whereby it could not definitely be determined in how far the total slip along the movement zone is due to pure material creep and/or accumulation of small shear slip movements on numerous discrete planes

5.4.3 Failure and temporal behaviour of sliding zone materials

Classical approaches to estimate the slope stabilities are based on the calculation of the safety factor, i.e. defined as the ratio between the driving and resisting forces. With this factor it is possible to estimate the present stability of a slope, even though time-dependant strength degradation processes are not considered. The shear strength of the sliding zone material, i.e. the resisting forces, is of decisive important for the determination of the stability conditions. A simple model for the estimation of the shear strength represents the Mohr-Coulomb model, which is based on two parameters only, the cohesion and the friction angle. These can be determined by means of triaxial compression or shear box tests in the laboratory.

Results of tests performed on different sliding zone materials, i.e. kakirite and glacial till samples, are given in Table 5.1 Irrespective of the applied laboratory testing method the friction angle of the material ranges between 31° and 39°, and the cohesion was found to be below 54 kN/m^2. Comparisons of these laboratory data with shear strength parameters obtained from back-calculations show that - for some investigated landslides - friction angles significantly below 31° and cohesions close to 0 are needed to induce slope failure. This discrepancy suggests that laboratory tests and in-situ back-calculation may differ due to scale effects, pore pressure influences and others.

Table 5.1 Mohr-Coulomb shear parameters of sliding zone samples

Sample number	Test type	Friction angle (°)	Cohesion (kN/m^2)
KG1	CD1	35,3	14,0
	RS-saturated	32,3	14,8
	RS-unsaturated	36,4	22,2
KG2	CD1	30,7	54,0
	RS-unsaturated	32,7	36,7
HM1-K	CD1	34,1	15,0
	RS-saturated	30,9	37,4
HM1-M1	CD1	36,0	18,0
	CD2	36,2	7,0
	RS-saturated	34,4	36,2
HM1-M2	CD1	39,1	24,0
	CD2	38,0	6,0
	RS-saturated	35,8	42,9

Samples KG1, KG2 and HM1-K: kakirite formed from paragneiss; samples HM1-M1 and HM1-M2: glacial till material from the sliding zone (see Figs. 5.7); CD: triaxial tests of cylinders with D x H = 10 x 20 cm (CD1) or 4 x 7.5 cm (CD2); RS: fully saturated and unsaturated shear box test.

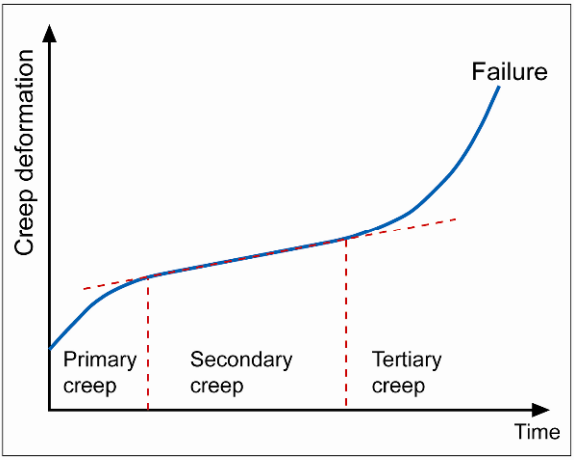

Fig. 5.9 Theoretical time-deformation behaviour (creeping) of material under constant stress

The deformation along an existing sliding zone is characterised by time-dependent processes such as material creep and/or friction along small-scale slip planes (Fig. 5.9). If creeping is the dominant mechanisms, the viscous deformation phase can be subdivided into three main regimes: primary, secondary and tertiary creep. So-called primary creep occurs simultaneously with the application of load and it is characterised by a monotone decrease in the creep rate. The secondary or steady-state creep is characterised by constant creep rates. If the loading is sufficiently high and enduring, an increase in the creep rate ensues until the material fails (tertiary creep).

The time-dependent (viscous) creep characteristics of sliding zone materials can be determined by laboratory tests. Therefore samples are loaded by constant stress over a longer period of time. Results from triaxial creep tests show that after consolidation under a defined stress condition all samples (approximately stationary) began to creep in a secondary manner (Fig. 5.10).

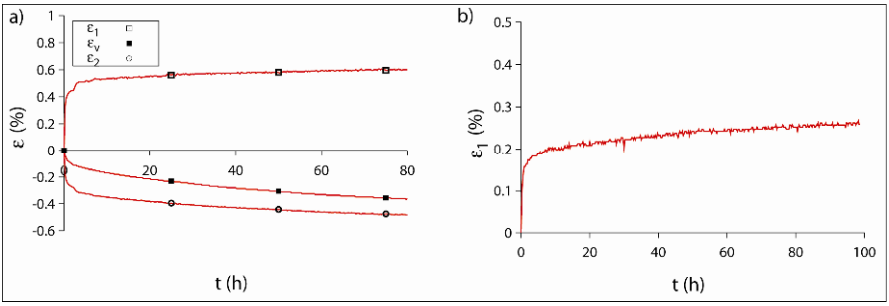

Fig. 5.10 Creep curves of a) a sample of glacial till material and b) a sample of kakirite rock

The evaluation of the laboratory tests was done with a linear-viscous and a non-linear-viscous model (Schneider-Muntau et al. 2006, Renk 2006), whereby the elastic deformations were analysed separately. In the case of the linear-viscous model according to Newton, for each test the viscosity of the material can be obtained from the applied stresses and the measured creep strain rates. The equivalent creep strain rate $\dot{\bar{\varepsilon}}$ can be determined from the strain rate tensor and the Mises equivalent stress from deviatoric stress tensor:

$$\dot{\bar{\varepsilon}} = \frac{1}{\eta}\bar{q} \qquad \text{(eq. 5.1)}$$

The assessment using a non-linear-viscous model was based on the following equation:

$$\dot{\bar{\varepsilon}} = \frac{1}{\eta}\left(\bar{q} - q_y\right)^n \qquad \text{(eq. 5.2)}$$

The crucial material parameters are the viscosity η, the yield stress q_y, which describes the stress state when the material begins to deform viscously, and the exponent n, that describes the non-linear behaviour. For the determination of these parameters several laboratory tests are needed. Based on the stress and creep strain rate of each single laboratory test a regression function can be calculated using the method of the least squares fit, which best describes the material behaviour according to the 3 parameters. For a non-linear-viscous model with n>1, the increase of the stress has a higher influence on the creep strain rate than in a purely linear-viscous model.

Seeing as triaxial tests only allow for relatively small displacements and strains, for the study of larger deformations ring shear experiments can be

conducted. In addition, laboratory tests always include scale effects, which need to be taken into account in the transferral to real models. Nevertheless geotechnical laboratory tests can contribute to a better understanding of the deformation processes along sliding zones.
Because there are parallels discernable in the movement patterns of active brittle fault zones with the formation of kakirites and sliding zones from landslides, frictional approaches from earthquake mechanics can be transferred to landslides. Thus, through the application of empirical material laws, such as the state- and velocity dependent friction laws (Ruina 1983, Dieterich 1992), it is possible to describe acceleration phases with subsequent stabilising or complete failure of slopes (Helmstetter et al. 2004).

5.4.4 Temporal deformation behaviour of landslides

Alpine regions are characterised by rock falls, topples, flows and slides with velocities ranging from several mm/a to several m/s. Slope instabilities that end in a sudden collapse show a deformation behaviour that depicts an accelerated velocity curve (Fig. 5.11). However, some landslides are characterised by a base activity superimposed by episodic phases of a higher slope velocities, which can be observed particularly in spring due to snow melting and rainfalls (Fig. 5.11). These phases of acceleration and stabilisation can presumably be ascribed to pore pressure fluctuations, to stabilising effects in the slope foot area and/or to changes in the material properties of the sliding zone itself.
Time series of deformation measurements from two cases studies show significant acceleration phases and periods of minor activity (Figs. 5.12 and 5.14). Remarkably, the velocities of low and high activity phases can differ about a factor of up to 8000, as was observed at the Steinlehnen rockslide (Zangerl et al. 2007; Figs. 5.13 and 5.14). There at the end of June and beginning of July 2003, a maximum slope velocity of over 4 m per day was measured here with a terrestrial laser scanner. After a one-month acute phase, whereby the trigger of this acceleration phase is still unknown, a continuous decrease of the velocity ensued (Fig. 5.14a). In spring 2004, once again there was a phase of acceleration with a maximum slope velocity of up to 4 cm per day (about a factor of 100 lower), which was followed by a deceleration to about 0.5 mm per day in the autumn of 2004 (Fig. 5.14b,c). Even the strong rainfall in August 2005 could not lead to a remarkably reacceleration of the sliding slab (Fig. 5.14b, Zangerl et al. 2007).

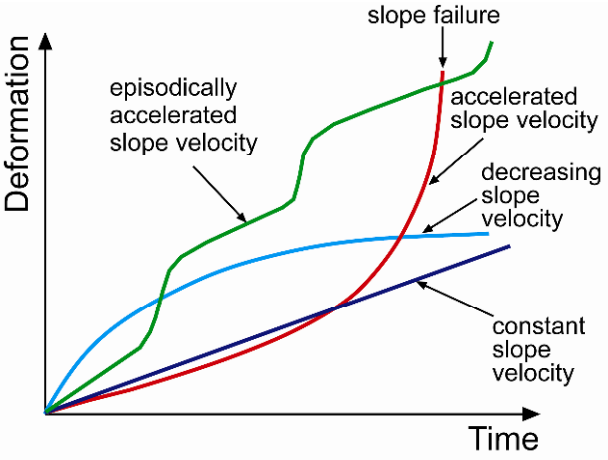

Fig. 5.11 Temporal deformation types: episodic accelerated velocity, constant slope velocity, decreasing slope velocity, accelerated slope velocity with failure (modified according to Keusen 1997)

Cyclical movements but in a much lower magnitude could also be observed at the Hochmais rockslide (Zangerl et al. 2007, Figs. 5.6 and 5.12). Exceptionally long time-series of about 40 years observation period show that the yearly slope velocity varies between 0.01 mm and 1 mm per day, i.e. a factor of 100. Every year an acceleration phase begins between January and March and lasts to the summer. This interval marks a period where precipitation in the form of rainfall does not occur. Instead, a regression analysis of the data together with that of the reservoir levels show a good temporal agreement between the slope velocity and the depletion of the Gepatsch reservoir (Figs. 5.7 and 5.12, Evers 2006, Zangerl et al. 2007). Hence for this case study the slope velocity is primarily influenced by the reservoir water level.

Similar velocity patterns, however not connected to reservoirs, could be observed at the landslides of La Clapière (France, Helmstetter et al. 2004), Triesenberg (Liechtenstein, Francois et al. 2006) or Gradenbach (Austria, Weidner 2000). On the basis of these case studies a relationship between hydrological or hydrogeological influence factors and slope activity could be shown.

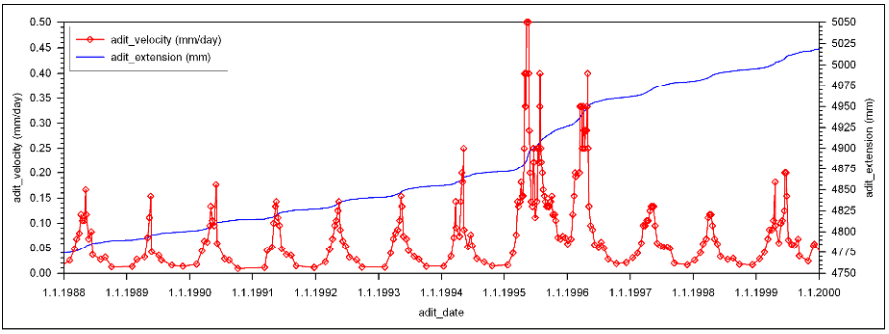

Fig. 5.12 Elongation of wire extensometer in the exploration adit I (see Fig. 5.6 and 5.7) and the derived velocity of the sliding slab Hochmais. The yearly acceleration phases occur in late winter and spring

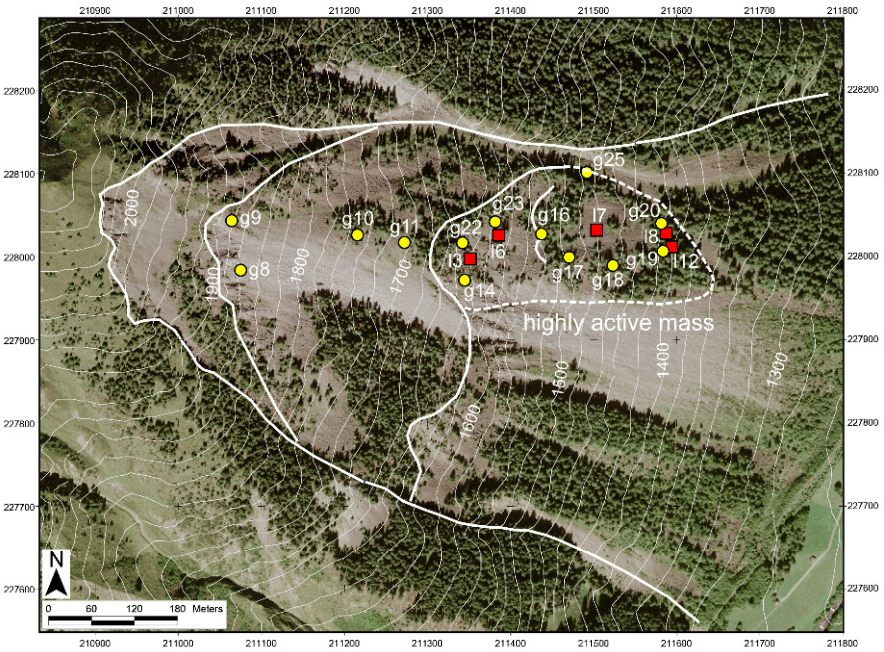

Fig. 5.13 Overview of the Steinlehnen rockslide system (Gries i. Sellraintal, Tyrol) with a highly active sliding slab (Ortho-image: TIRIS Land Tirol). Red squares = laser scanner windows, yellow points = terrestrial survey points, measured from the opposite slope (cf. Fig. 5.14). The complete rockslide system shows a difference in height of about 800 m and a thickness of about 70 m. The highly active sliding mass reaches a thickness of about 20 m. The discontinuities which may induce these slope failures are not the foliation and compositional layering dipping flat into the slope, but one of the main fracture sets dipping moderately inclined down the slope

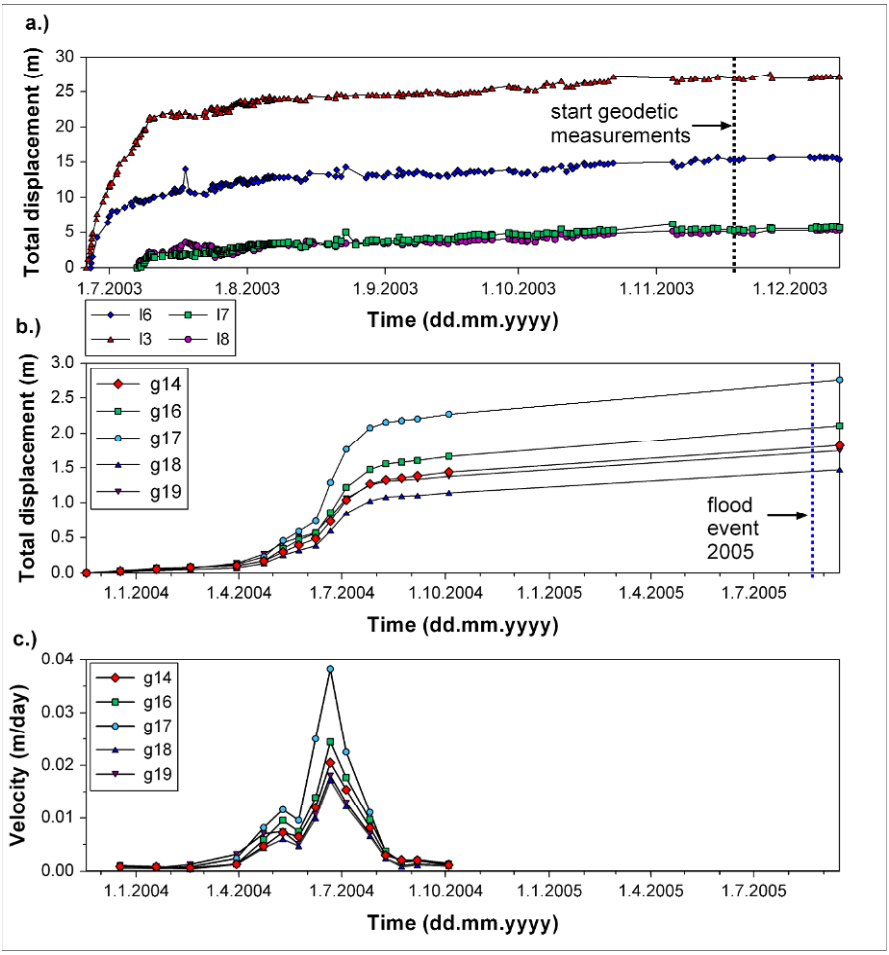

Fig. 5.14 Deformation monitoring of the highly active sliding slab Steinlehnen (cf. Fig. 5.13): a) total displacement of laser scanner windows measured from the opposite slope, b) total displacement of triangulation points measured from the opposite slope, and c) derived velocity pattern of triangulation points

5.5 Geophysical investigation methods

5.5.1 Active seismic methods

Active seismic methods can be applied to investigate the geometry, internal structure and material parameters, e.g., landslide thickness and boundaries, the basal sliding zone, degree of fracturing, sliding mass porosity (Brückl 2006). The objective of all active seismic methods focuses on the determination of the seismic velocity field in the subsurface through analysis of the wave propagation. The seismic velocity is related to the mechanical parameters of the rock mass, especially to the bulk modulus, shear modulus and the density (Ewing 1957).
Seismic waves can be generated with hammers, mechanically or pneumatically accelerated drop weights, vibrators or detonating explosives. The recording of the seismic waves can be done via geophones in a linear (2-D seismology) or an areal arrangements (3-D seismology). The signals of the geophones are stored in a portable registration unit. Given that the propagation of seismic waves represents an extremely complex process, several different seismic methods that focus on different types of waves are available (Kearey 2002). The three most important methods are described in the following paragraph:

a) Seismic reflection concentrates on the measuring and processing of seismic waves, which are reflected at boundaries characterised by a change of seismic impedance (i.e. the product of seismic wave velocity and density). Reflected waves never appear as first breaks; therefore an appropriate data acquisition and processing must be applied to extract these signals from the entire wave field. Most of the different reflection processing techniques (e.g. static correction, spike deconvolution, bandpass filter, NMO-correction, CDP-stacking, migration) were developed for the hydrocarbon exploration industry (Yilmaz 1987) and then transferred to engineering and environmental related tasks.

b) Seismic refraction is based on the analyses of critically refracted seismic waves, which appear as first breaks in the seismogram. Since the first breaks are clearly detectable, data acquisition and evaluation of signals is easier and less influenced by geological conditions. Data processing of seismic refraction measurements can be done based on different methods such as picking of first breaks, delay-time method and time to depth conversion. Hence a layered model characterised by a step-like velocity-depth function will be obtained. The fundamental condition that critically re-

fracted seismic waves can occur in a rock or soil is related to the seismic behaviour of the refractor. A seismic velocity of the refractor higher than the velocity of the overlaying layer should be given. In contrast to seismic reflection, velocity inversions (with an increase of depth) can not be resolved. Even though the penetration depth of seismic refraction is smaller than that of seismic reflection, the former provides better resolution of the velocity field.

c) Seismic tomography is based on the travel times of transmitted waves. These travel times contain integral information about the velocity along the seismic ray. Generally, the standard measurement geometry applied to seismic tomography is performed between two boreholes. Nevertheless the principles can also be transferred to surface investigations (seismic refraction tomography). This method is also based on observation and processing of the travel times of first breaks. Seismic tomography needs a continuous increase of the velocity with depth, because only then waves are able to return back to the surface (geophone). In spite of this basic condition, velocity inversions are possible under certain circumstances. The data processing (picking of first breaks, forward modelling with a initial velocity field, wave front inversion) results in a spatially distributed velocity field. The resolution of the tomographic method depends on the quantity of rays penetrating the subsurface and their direction. In the ideal case the rays cover directions from 0° to 180° in relation to the surface.

For the seismic methods, the penetration depths, the resolution of velocity and depth, and the accuracy mostly depends on the measuring geometry (geophone distance, profile length) and on the frequency domain of the source and the geophones. The penetration depth for seismic refraction is 1/4 to 1/3 of the total profile length and therefore the geophone distance is normally larger than for the seismic reflection, where the penetration depth is mainly influenced by the strength of the source and the subsurface velocity field. In order to get a good resolution a small geophone distance should be applied. The frequency domain of the seismic measurements also restricts the resolution, because the wavelength of the seismic wave is a product of the frequency and the velocity. So the size and thickness of a structure must be adequately large to be resolved. In general, for all methods it can be said that the velocity and depth can be determined with an accuracy of 15-20%. The classic seismic survey is performed along 2-D profiles, whereby subsurface mapping of complex 3-D structures remains difficult. For this reason an increasing number of 3-D seismic surveys were carried out, particularly in oil field exploration.

In the Tyrol a 3-D refraction seismic survey was carried out to explore the thickness and internal structure of the large-scale Niedergallmigg - Matekopf rockslide (Fig. 5.15, Chwatal et al. 2005, 2006). The upper part of the sliding mass is composed of paragneisses and schists, which were thrust on phyllitgneisses, phyllites and amphibolites that are encountered at the middle and lower part of the slope (Kirschner and Gillarduzzi 2005). Morphological features, in particular the size of the main scarp, indicate a total displacement of about 180 m. Results from geodetic measurements show annual surface displacements ranging between 5 to 10 centimetres for the active sliding mass.

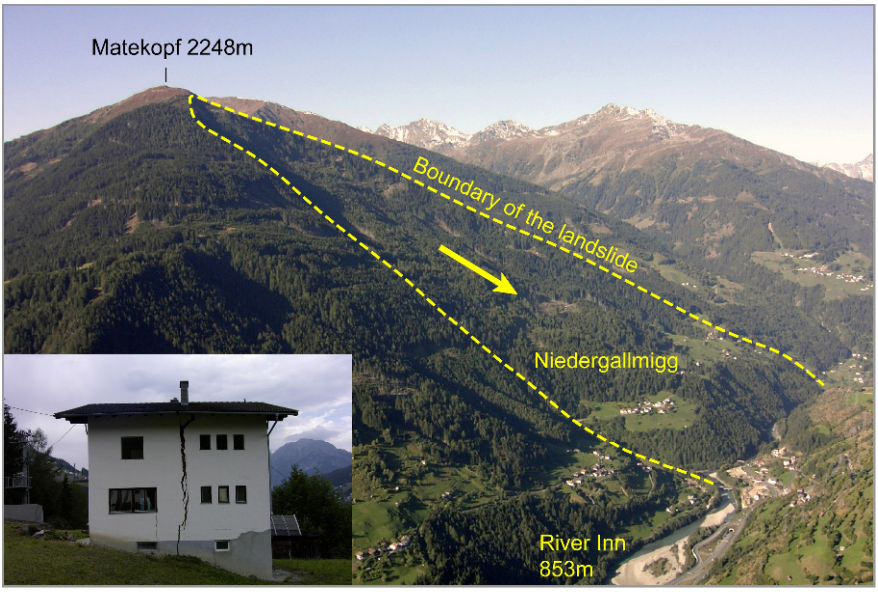

Fig. 5.15 View of the Niedergallmigg-Matekopf landslide. Insert shows movement induced fracturing of a house on the landslide

In order to perform the 3-D refraction seismic survey 373 seismic stations were installed along 4 profiles comprising a total length of 7.5 km and a geophone distance of 15-25 m. 41 shots were recorded simultaneously by all receivers. This geophone set up enabled a 2-D analysis along the 4 profiles but also a 3-D inversion of the whole data set (inline and cross-line shots).

The seismic data show a vertical gradient of the velocity for the sliding mass and a nearly constant velocity for the underlying compact rock. Therefore, a combination of seismic refraction tomography for the landslide mass and standard seismic refraction method for the compact rock

were applied. In order to analyse the measured data, 3-D processing techniques described by Brückl et al. (2003) and tomographic inversion algorithm published by Hole (1992) were used. As a result, the 3-D seismic velocity distribution of the landslide system and its stable surrounding is gained.

The P-wave velocities of the sliding mass are near the surface 1000-2000 m/s, at depths of 25-150 m 2000-3000 m/s and below 150 m 3000-4000 m/s. Further below velocities of 4800-5200 m/s were measured, which can be interpreted as the basis of the landslide (Fig. 5.16).

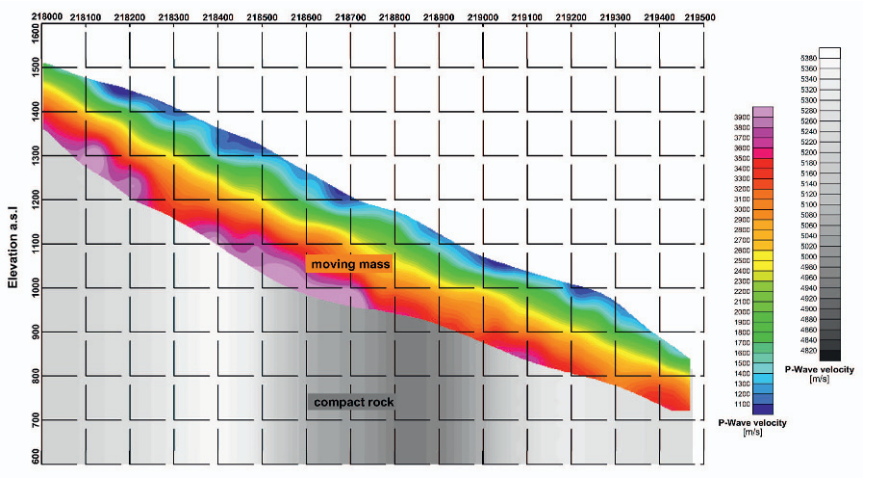

Fig. 5.16 S-N section of the 3-D velocity field of the Niedergallmigg-Matekopf landslide

Based on the seismic results a geometrical model showing the spatial thickness distribution of the Niedergallmigg-Matekopf landslide was constructed, featuring a maximum thickness of 320 m and a volume of 0.43 km^3 (Fig. 5.17). At the lateral boundaries, i.e. areas yielding little seismic information, morphological observations (e.g. scarp features) were added to establish the geometrical model. In addition, in areas without seismic data i.e. the upper region of the landslide, an interpolation technique was used.

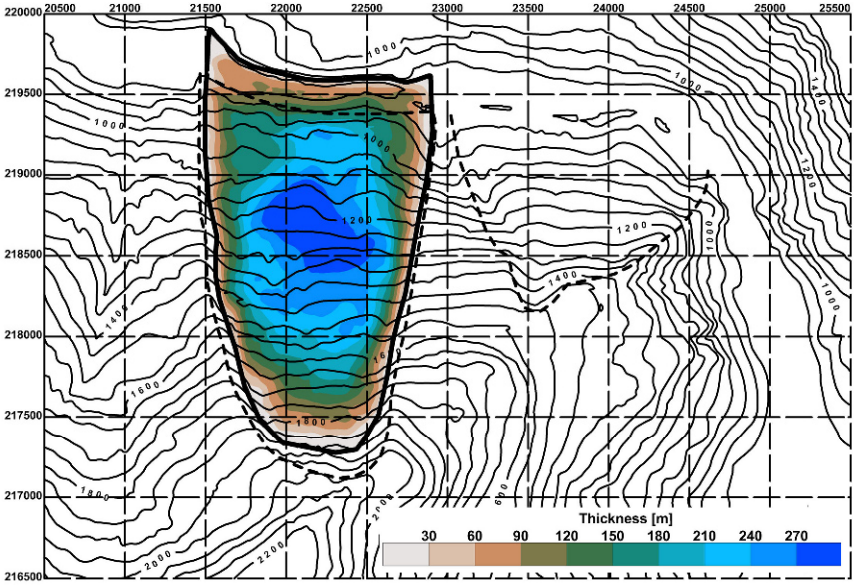

Fig. 5.17 Thickness map of the Niedergallmigg-Matekopf landslide

Plotting the P-wave velocities of the sliding mass versus depth an average velocity depth function that is based on the assumption of dry or drained slope conditions (Brückl and Parotidis 2005) can be fitted. The porosity of the fractured rock mass may be estimated from a relationship according to Gassmann (1951) and Watkins et al. (1972) and is based on P-wave velocities. For the Niedergallmigg-Matekopf landslide an average creeping rock mass porosity of 0.21 was estimated (Fig. 5.18)

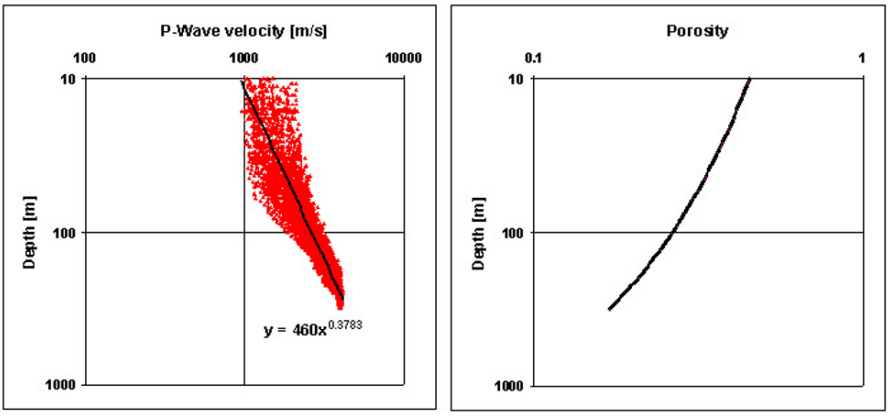

Fig. 5.18 Velocity-depth and derived porosity-depth function of the Niedergallmigg-Matekopf landslide

5.5.2 Ground Penetrating Radar

Ground Penetrating Radar (GPR) systems enable quick and non-destructive field explorations to depths of some tens of metres and were, in the Eastern Alps, already applied to rock-glaciers and water-unsaturated talus-deposits (e. g. Sass and Wollny 2001, Krainer et al. 2002). Now GPR measurements were successfully taken for near-subsurface investigations at different accumulation areas of fossil landslide deposits to analyse their thickness, internal structure and spatial distribution. Field surveys were carried out off-road at two lithologically different sites in Tyrol (Austria): firstly, at a rockslide in the Ötztal basement complex, and secondly, in the Northern Calcareous Alps at medial to distal accumulation areas of the prominent Fernpass rockslide. System parameters, measurement modes and data processing are documented in Prager et al. (2006).
Based on detailed field studies and drilling campaigns, at Fernpass down to depths of 14 m, the processed and topographically corrected GPR data can be well attributed to different depositional units. At both sites, the radargrams show several distinct reflectors with varying intensities and geometries, extending to depths of at least 20-30 m. Remarkably, the radar signals were not effectively shielded by the shallow-seated groundwater table, but penetrated down into deeper parts of the water-saturated rockslide deposits and their substrate. The combined field and subsurface data indicate that the distal Fernpass rockslide deposits spread upon groundwa-

ter-saturated, fluvio-lacustrine sediments and show strong variations in thickness. Measurements taken at a distance of about 11 km from the uppermost scarp area, clearly point to a maximum thickness of the distal slide debris of approx. 20-30 m. As a further result, the Toma, i.e. cone-shaped hills composed of rockslide debris, show deeper roots than the topographically less elevated rockslide deposits between them. These undulating basal reflectors indicate subsidence of the rockslide debris into the fine-grained substrate due to loading; a distinct sub-planar sliding plane is not detectable here. Further GPR measurements were taken at an alluvial plain, which is situated on top of the medial Fernpass rockslide deposits. Here the processed radargrams clearly show an on-lap of prograding debris flows onto the hummocky rockslide relief, a geometry which correlates well with the field situation and drilling data. Furthermore, the internal stratification of the fluvial debris is best recognisable in the radargrams and demonstrates the high resolution of the applied GPR system. Therefore, this is a useful tool to explore near-subsurface structures, even in groundwater-saturated environments and hardly accessible study-areas.

5.6 Monitoring of landslides

Even though falls, rapid topples and slides may occur seemingly unexpected and suddenly, such events are nearly always characterised by long-term preparation phases. The cause for pre-failure deformation can be found in the physical properties of soil and rock masses, which are able to accumulate elastic and plastic deformation before failure occurs. This characteristic material behaviour enables the application of monitoring and warning systems with the aim of an early detection of possible slope failure. In addition, surface and subsurface deformation monitoring of landslides are absolutely essential for the development of kinematic models.
Classic monitoring systems are based on the recordings of displacements and strains on the surface or in the depths of the landslides. In addition new monitoring systems based on micro seismic activity have been developed. These systems measure the seismic energy released through fracture and deformation processes within a landslide.

5.6.1 Deformation Monitoring

Deformation measurements aim to determine the kinematics and temporal velocity behaviour of unstable slopes. Although field observations can provide indications of the current movement status of a landslide, the ques-

tion whether a slope is currently stabilised or moving can only be definitely answered with deformation measurements. Landslide deformation measurements provide data for the spatial distribution, orientation and magnitude of the displacement vectors on surface and subsurface and the temporal and spatial variation of slope velocities. Based on surface deformation data a spatial differentiation between stable bedrock units and active sliding masses as well as between variable active sub-slabs can be performed. These data are useful for the determination of the temporal slope activity, the landslide kinematics and the acceleration/trigger factors. In general, deformation measurements also form the basis for slope stability forecasts. The resulting difficulties in regard to the temporal development of a slope can clearly be seen in Fig. 5.11. This is especially the case for the prognosis of episodically accelerated slope velocities with a relatively linear base trend. In contrast, for accelerated slope velocities the trend and time of failure are easier to predict.

Slope deformation can be monitored a) pointwise, b) linewise and c) areal and can be measured in-situ and/or by remote sensing methods. Point data can be obtained through triangulation (x,y,z-coordinates), levelling (vertical z-coordinate), global positioning system (GPS, x,y,z-coordinates), wire extensometer (distance between 2 points), joint- or crackmeter (distance between 2 points), laser distance meter (distance between 2 points) and water level gauge measurements (vertical z-component between 2 points). Line data are the result of inclinometer measurements (Willenberg 2004), some types of extensometer- (Krähenbühl 2004) and Trivec measurements (Kovari 1988). Areal information about the deformation field on the surface of a landslide can be obtained by photogrammetry (Casson et al. 2003), terrestrial or satellite based radar interferometry (Rott et al. 1999, Fig. 5.19) and terrestrial or airborne laser scanning (Scheikl et al. 2000, Kemeny et al. 2006, Figs. 5.13 und 5.14).

Crucial parameters when planning a slope monitoring system are a) the number of observation points that are needed to monitor the whole landslide, b) the size and boundaries of a landslide, and c) the expected slope velocity and hence the required accuracy of the measurement method. Furthermore, it must be clarified in how far surface observations are representative for the understanding of landslide kinematics or whether borehole data (inclinometers) are needed to obtain the internal deformation behaviour. Moreover, the accessibility of the measuring area is decisive for the choice of an appropriate system. The frequency of the measurement campaigns should be defined when working with an episodical type of monitoring set-up. First evidences of the spatial distribution of slope deformation and its velocities may be given by structural and geomorphological features (open cracks, vegetation markers, etc.). Based on these field ob-

servations and the estimated slope velocity the time span between the first and second measuring campaign is defined. Subsequent monitoring data can be used to refine the measuring interval. At some landslides with high risk potential it is essential to install permanent monitoring systems that are able to record slope displacements continuously. Usually such monitoring systems can be upgraded with automatic warning devices, which set off an alarm when a predefined velocity threshold is reached.

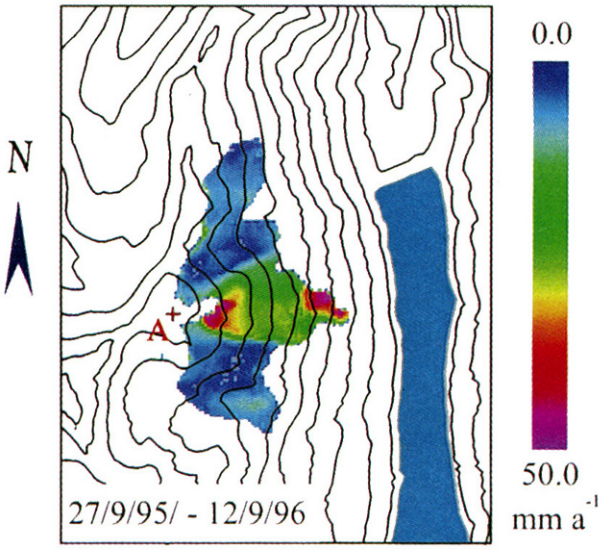

Fig. 5.19 Surface velocity pattern (mm/a) of the Hochmais-Atemkopf rockslide (Kaunertal, Tyrol), derived from radar interferogramms from 27.09.1995 and 12.09.1996. In the lower region of the slope no velocity values could be obtained due to forestation (from Rott et al. 1999)

The displacement vectors of points can be measured in form of absolute and relative coordinates. Absolute coordinates may be gained from Global Positioning Systems (GPS) and geodetic terrestrial methods. Latter may also be applied for relative displacement measurements between stable reference points outside and unstable points on the landslide (Fig. 5.20). This measurement configuration helps to avoid large measuring distances and height differences and therefore yields highly accurate measurement data. Other relative displacement measurements may result from wire extensometer or joint-meter installations. Given that these methods can only measure the distance between two points, a check by means of terrestrial

geodetic methods to obtain the 3-D displacement vector of the stable and unstable point is necessary to avoid misinterpretations.

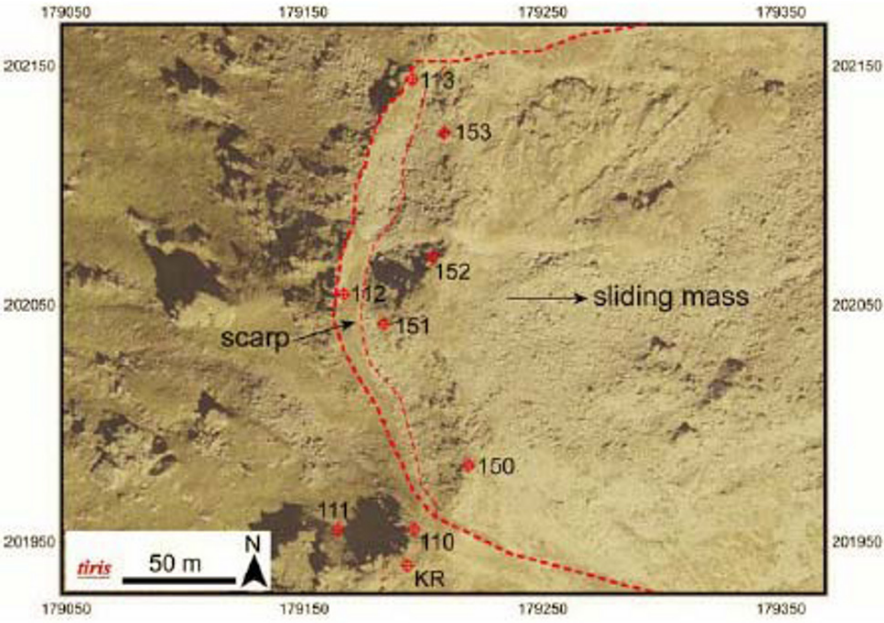

Fig. 5.20 Relative monitoring network around a mountain ridge to detect the rockslide activity (Kreuzkopf, Tyrol). Whilst the monitoring points 110, 111, 112, 113 are assumed to be stable, the points 150, 151, 152, 153 are on the sliding mass. Through the relatively short distance of less than 100 m and the minor height difference of less than 40 m possible displacements can be achieved with an accuracy of less than 2 mm (Orthofoto: Tiris Land Tirol)

For any deformation and risk analyses, data of the temporal variation of slope velocities are essential. In order to determine this, the measured displacement values must be numerically differentiated over time. The data thus obtained can be plotted in a velocity versus time diagram, whereby the velocity represents a derived value. Differential values such as the velocity of slope points are error-prone, especially when data points are temporally close together. Considering this and the fact that monitoring points contain a measurement error, the differentiation of such data sets can lead to great fluctuations in the calculated velocities. For example laser scanner raw data (Fig. 5.14a) from the Steinlehnen rockslide yielded widely scattering slope velocities, because of the relatively large measurement error and the high frequency of measurement campaigns. In order to avoid unrealistic velocity pattern fluctuations, a) the displacement curves may be

smoothed out, b) the time intervall between measurement campaigns for differentiation may be increased and/or c) more accurate measurement methods such as terrestrial geodetic surveys may be applied. Based on precise triangulation measurements performed monthly at the Steinlehnen rockslide it was possible to calculate a velocity-time curve (Fig. 5.14b,c).

5.6.2 Seismic monitoring

Slope movements are characterised by the formation of new and coalescence of brittle fractures in the sliding mass and active sliding zones and presumably by "stick-slip" movements on existing shear planes. These fracturing and failure processes induce seismic energy that can be measured with a seismic monitoring network. The seismic events ("microearthquakes") can be analysed to determine the magnitude and source location of brittle deformation.

Since 2001 regular seismic monitoring campaigns were conducted on the deep-seated rockslides in Gradenbach (Carinthia, Austria) and Hochmais-Atemkopf (Tyrol, Austria). In 2005 the monitoring campaign was extended to the large-scale Niedergallmigg-Matekopf landslide (Fig. 5.15). Analyses of these monitoring data led to the design of a monitoring network which focused particularly on the observation of deep-seated mass movements (Fig. 5.21). The basic problems, when applying microseismic monitoring to landslides are: a) the signal strength of the events caused by landslides is usually very weak, b) settlements and infrastructure generate a high seismic noise level and c) there is still a lack of knowledge about the characteristic of the expected microseismic events.

Overall geophones register a variety of events (local earthquakes, events created by humans), that can not easily be classified due to their waveform and frequency characteristics. In order to allocate seismic events to landslides, the monitoring network should not only cover the landslide mass itself but also the surrounding areas (Fig. 5.21). Moreover, the seismological observation stations surrounding the landslide should be incorporated in the monitoring network.

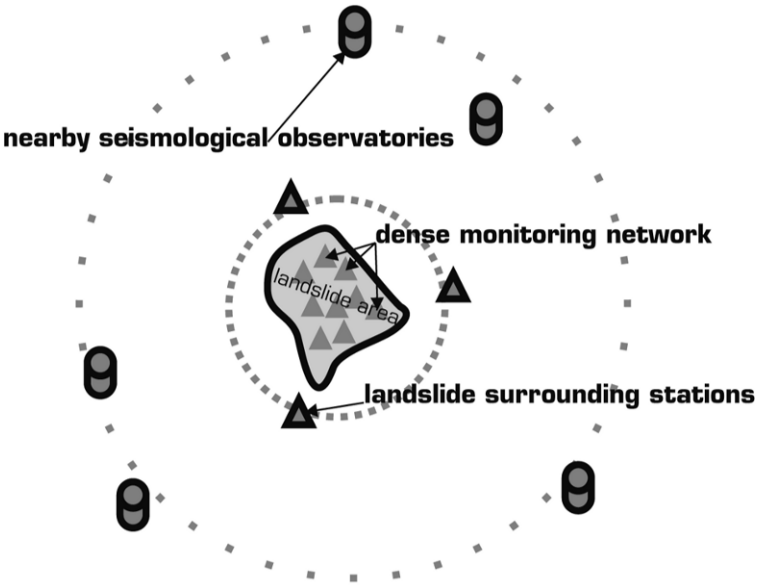

Fig. 5.21 Schematic set-up of a monitoring network for the observation of deep-seated landslides

Currently there is not enough information available about the characteristics of such landslide-induced seismic events (frequency pattern, wave form, duration of an event) to search specifically in the recorded data set. For the detection of events already known signals such as human generated „noise“ as well as global, regional and local earthquakes are eliminated from the data. The remaining signals that can not be assigned to any of the known types of events are classified as “interesting”. Earthquake catalogues and the surrounding seismological observatories aid in making a distinction between global, regional and local earthquakes. Spectro- and sonograms are used to detect weak signals and to visualise the frequency content (Joswig 1990). Different algorithms such as STA/LTA (Allen 1982, Allen 1978) and Principle Component Analysis (Magotra 1987, Wagner 1996) were tested for their automatic detection of events. The sensitivity of these detectors has to be adjusted to a very high level to be able to also detect weak events. This high sensitivity causes a great number of “error detections”. For an improved and automatic detection of events “pattern recognition algorithms” can be applied (Joswig 1990). The disadvantage of these algorithms is that a profound knowledge about the fre-

quency characteristics of the interesting events is presupposed, however, is currently unavailable.
The localisation of the events is an important indicator of whether a registered event is a micro-earthquake induced by landslides. For "interesting" events, showing a sufficient signal-noise-ratio, localisation can be conducted with the help of first arrival travel times and a 3-D P-wave velocity model. Using the NonLinLoc software the source coordinates can be determined (Podvin and Lecomte 1991, Lomax et al. 2005). This localisation method was tested with controlled seismic sources i.e. dynamite detonations at the study site Hochmais-Atemkopf and shows that through a 3-D velocity model reliable results can be achieved (Fig. 5.22). Generally it was found that localisation of the epicentre in regard to a transferred coordinate system parallel to the slope inclination are easier to determine than the focal depth.

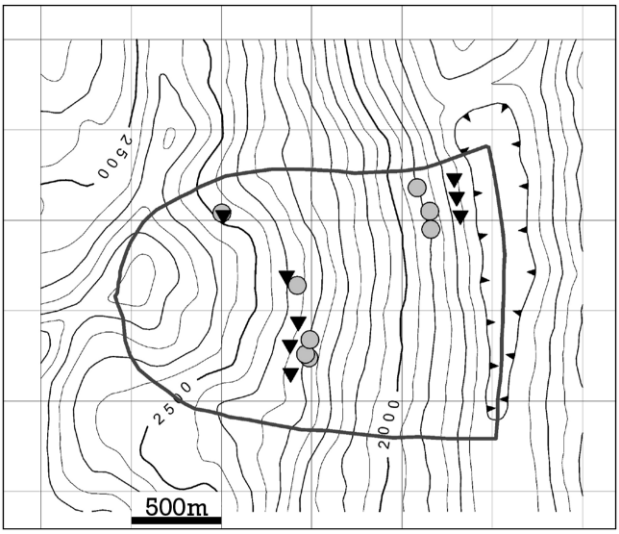

Fig. 5.22 Re-localisation of the detonations of the measurement campaign Hochmais-Atemkopf (Kaunertal, Tyrol). Black triangles = actual detonation points, grey circles = re-localised detonations

Currently there is not enough information available about the characteristics of such landslide induced events (frequency pattern, wave form, duration of an event) to search specifically in the recorded data set

However, events with low signal-noise ratio or emerging energy cannot be detected by standard detection and localization routines. Spectrogram and image processing routines are used to automatically detect and classify the

recorded seismic events. Localization routines based on amplitude distribution are used to localise events with no clear first P-wave arrival (Mertl and Brückl 2007). Many events that could be classified as micro-earthquakes exhibit composite or multi-event characteristics. Such events were observed on all three examined slopes (Fig. 5.23). The total duration of micro-earthquakes lies between 5-20 seconds, whereby the main part of the frequency content is <30 Hz. The later events of a composite micro-earthquake mostly exhibit a lower frequency content than the primary event.

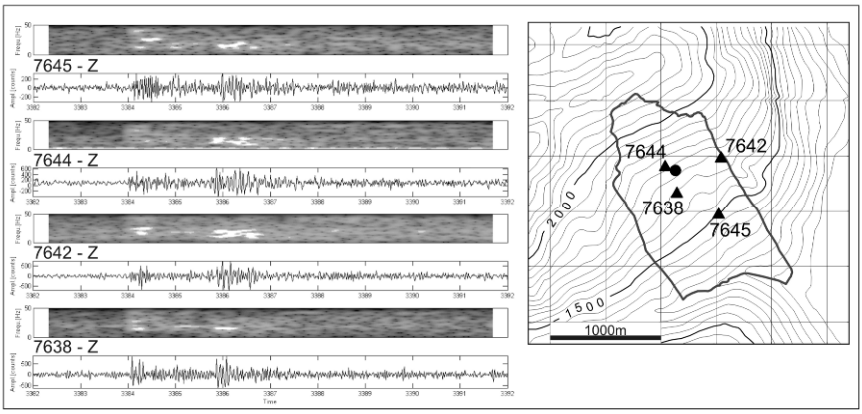

Fig. 5.23 Typical registration of a multi-event microearthquake, recorded on the landslide Gradenbach

Besides the composite and multi-events other types i.e. narrow frequency-band and low-frequency events were recorded on the three slopes. However, these could not distinctly be classified as landslide induced events. Figure 5.24 depicts an example of such a “narrow frequency” event.

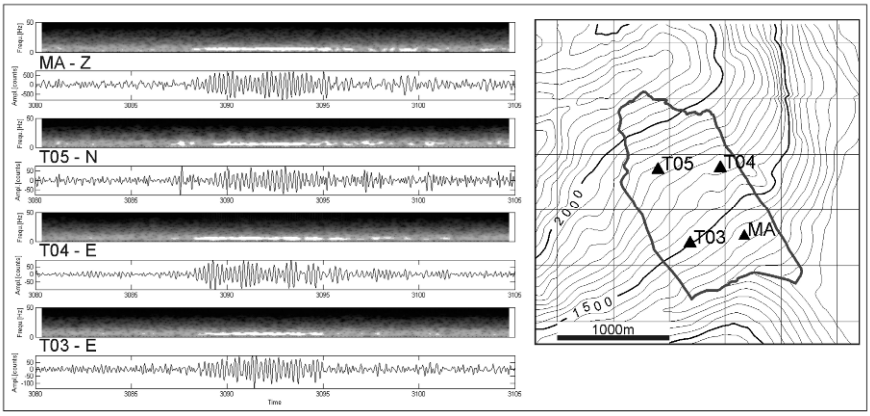

Fig. 5.24 Typical registration of a narrow-frequency event, recorded on the landslide Gradenbach

5.7 Summary

The complexity and variability of diverse kinematical landslide types requires multi-disciplinary approaches to analyse the underlying processes and mechanisms. Therefore disciplines from the field of geotechnics, geology, geomorphology, geodetics and geophysics should ideally interact to reach a high level of knowledge.

Age dating of fossil landslides helps to resolve the temporal and spatial interrelationship of slope instabilities in different geological settings and under different climatic conditions in the Holocene. Time periods of increased slope activity can be resolved and linked to feasible triggers. Analysis of age dating results shows that in several cases reactivation or multiple failures on sites occurred in the past. Thus an increasing compilation of landslide events from the past can provide data to establish probability-based estimations of the occurrence of slope failures for a given area. Such data are needed as input for further risk analyses approaches.

Fundamental principles from fracture and friction mechanics and material creep laws help to understand slope deformations in a kinematical, mechanical and temporal manner. Both the triggers that induce slope failures or accelerations and the factors which lead to slope stabilisation require detailed investigation and analyses to establish reliable forecasts. In addition the physical comprehension of slope failures and deformation processes provide the basis for the development and planning of monitoring systems, in-situ investigation methods and stability analyses based on limit equilib-

rium methods or numerical modelling approaches. Monitoring of landslide deformation and microseismic activity provide crucial information about the kinematics and the temporal deformation behaviour.

References

Abele G (1974) Bergstürze in den Alpen. Ihre Verbreitung, Morphologie und Folgeerscheinungen. Wiss. Alpenvereinshefte, München 25, pp 1-230

Allen R (1978) Automatic earthquake recognition and timing from single traces. Bulletin of the Seismological Society of America 68(5), pp 1521-1532

Allen R (1982) Automatic phase pickers: their present use and future prospects. Bulletin of the Seismological Society of America 72(6), pp 225-242

Amann F (2006) Großhangbewegung Cuolm da Vi (Graubünden, Schweiz). Geologisch-geotechnische Befunde und numerische Untersuchungen zur Klärung des Phänomens. Dissertation, Friedrich-Alexander Universität Erlangen-Nürnberg, p. 206

Atkinson BK (1984) Subcritical crack growth in geological materials. Journal of Geophysical Research 89(B6), pp 4077-4114

Atkinson BK (1987) Introduction to fracture mechanics and its geophysical applications. In: Atkinson BK (ed), Fracture mechanics of rock, Academic Press, pp 1-26

Azzoni A, Chiesa S, Frassoni A, Govi M (1992) The Val Pola Landslide. Engineering Geology 33, pp 59-70

Brückl E, Brückl J (2006) Geophysical models of the Lesachriegel and Gradenbach deep-seated mass movements (Schober range, Austria). Engineering Geology, 83(1-3), pp 254-272

Brückl E, Parotidis M (2005) Prediction of slope instabilities due to deep-seated gravitational creep. Natural Hazards and Earth System Sciences 5, pp 155-172

Brückl E, Zangerl C, Tentschert E (2004) Geometry and deformation mechanisms of a deep seated gravitational creep in crystalline rocks. In.: Schubert (ed), Proceedings EUROCK 2004 & 53rd Geomechanics Colloquium, pp 229-230

Brückl E, Behm M, Chwatal W (2003) The application of signal detection and stacking techniques to refraction seismic data. Oral Presentation at AGU, San Francisco, 08-12 December 2003

Cappa F, Guglielmi Y, Soukatchoff VM, Mudry J, Bertrand C, Charmoille A (2004) Hydromechanical modeling of a large moving rock slope inferred from slope levelling coupled to spring long-term hydrochemical monitoring: example of the La Clapière landslide (Southern Alps, France). Journal of Hydrology 291(1-2), pp 67-90

Casson B, Delacourt C, Baratoux D, Allemand P (2003) Seventeen years of the ‘‘La Clapière’’ landslide evolution analysed from ortho-rectified aerial photographs. Engineering Geology 68, pp 123-139

Chwatal W, Kirschner H, Brückl E, Zangerl C (2005) Geology and 3D seismic structure of the Niedergallmigg-Matekopf mass-movement, Tyrol, Austria. EGU 2005, Wien, Geophys. Res. Abst. 7, 02566

Chwatal W, Kirschner H, Brückl E, Zangerl C (2006) Kinematics and Hazard of the Niedergallmigg-Matekopf mass movement. EGU 2006, Wien, Geophys. Res. Abst. 8, 05998

Cruden DM (1991) A simple definition of a landslide. Bulletin International Association for Engineering Geology 43, pp 27-29

Cruden DM, Varnes DJ (1996) Landslide Types and Processes. In: Turner AK, Schuster RL (ed) Landslides: investigation and mitigation (Spec. Rep. 247), National Academy Press, Washington D.C., pp 36-75

Dapples F, Oswald D, Raetzo H, Lardelli T, Zwahlen P (2003) New records of Holocene landslide activity in the Western and Eastern Swiss Alps: Implication of climate and vegetation changes. Ecl. Geol. Helv. 96, pp 1-9

Dieterich J (1992) Earthquake nucleation on faults with rate- and state-dependent strength. Tectonophysics 211, pp 115-134

Eberhardt E, Stead D, Coggan JS (2004) Numerical analysis of initiation and progressive failure in natural rock slopes-the 1991 Randa rockslide. Int. J. Rock Mech. Min. Sci. 41, pp 69-87

Einstein HH (1993) Modern developments in discontinuity analysis - the persistence-connectivity problem. In: Hudson JA (ed) Comprehensive Rock Engineering, Volume 3, Pergamon Press, Oxford, pp 193-213

Einstein HH, Stephansson O (2000) Fracture systems, fracture propagation and coalescence, Issue Paper, Proc. GeoEng 2000, Melbourne

Einstein HH, Veneziano D, Baecher GB, O'Reilly KJ (1983) The effect of discontinuity persistence on rock slope stability. Int. J. Rock Mech. Min. Sci. Geomech. Abstr. 20(5), pp 227-236

Evers H (2006) Geodätisches Monitoring und einfache statistische Auswertungsmöglichkeiten für Massenbewegungen an Hängen. Master Thesis, HTWK Leipzig, p 118

Ewing WM, Jardetzky WS, Press F (1957) Elastic waves in layered media, Mc Graw-Hill Book Company, New York

François B, Tacher L, Bonnard Ch, Laloui L, Triguero V (2007) Numerical modelling of the hydrogeological and geomechanical behaviour of a large slope movement: the Triesenberg landslide (Liechtenstein). Canadian Geotechnical Journal 44, pp 840-857

Gassmann F (1951) Über die Elastizität poröser Medien. Vierteljahrsschrift der Naturforschenden Gesellschaft in Zürich 96(1), pp 1-23

Geyh MA, Schleicher H (1990) Absolute age determination: physical and chemical dating methods and their application. Springer, p 503

Helmstetter A, Sornette D, Grasso JR, Andersen JV, Gluzman S, Pisarenko V (2004) Slider block friction model for landslides: Application to Vaiont and La Clapière landslides. Journal of Geophysical Research 109(B02409), pp 1-15

Henzinger J (2005) Massenbewegung Steinlehne-Gries im Sellrain. In: Heissel G, Mostler H (ed) Geoforum Umhausen Band 3, pp 71-82

Hermanns RL, Blikra L H, Naumann M, Nilsen B, Panthi KK, Stromeyer D, Longva O (2006) Examples of multiple rock-slope collapses from Köfels (Ötz valley, Austria) and western Norway, Engineering Geology 83, pp 94-108

Heuberger H (1966) Gletschergeschichtliche Untersuchungen in den Zentralalpen zwischen Sellrain und Ötztal. Innsbruck, Wiss. Alpenvereinshefte 20, 1-126

Hole JA (1992) Nonlinear high-resolution three-dimensional seismic travel time tomography. Journal of Geophysical Research 97, pp 6553-6562

Hudson JA, Harrison JP (1997) Engineering rock mechanics. Elsevier Science Ltd., UK, p. 444

Ivy-Ochs S, Heuberger H, Kubik PW, Kerschner H, Bonani G, Frank, M, Schlüchter C (1998) The age of the Köfels event. Relative, 14C and cosmogenic isotope dating of an early Holocene landslide in the Central Alps (Tyrol, Austria). Zs. Gletscherkd. Glazialgeol. 34 (1), pp 57-68

Jerz H, v. Poschinger A (1995) Neueste Ergebnisse zum Bergsturz Eibsee-Grainau. Geol. Bavarica 99, pp 383-398

Joswig M (1990) Pattern Recognition for earthquake detection. Bulletin of the Seismological Society of America 80(1), pp 170-186

Kearey P (2002) An introduction to geophysical exploration, Brooks und I. Hill, p 262

Kemeny J (2003) The Time-Dependent Reduction of Sliding Cohesion due toRock Bridges Along Discontinuities: A Fracture Mechanics Approach. Rock Mechanics Rock Engineering 36 (1), pp 27-38

Kemeny J, Norton B, Turner K (2006) Rock Slope Stability Analysis Utilizing Ground-based LIDAR and Digital Image Processing. Felsbau 24(3), pp 8-15

Keusen HR (1998) Warn- und Überwachungssysteme (Frühwarndienste), Fan-Forum, Zollikofen, 1-40

Kirschner H, Gillarduzzi K (2005) Geodätisches Monitoring und Modellierung instabiler Hänge. In: Chesi G,Weinold T (ed) Internationale geodätische Woche Obergurgl 2005, Austria, pp 193-197

Kovári K (1988) General report: Methods of monitoring landslides. In: Bonnard C. (ed), Land-slides, Proceedings of the 5th International Symposium on Landslides, Lausanne, Switzerland, Balkema, Vol 3, pp 1421-1433

Krähenbühl R (2004) Temperatur und Kluftwasser als Ursachen von Felssturz. Bull. Angew. Geol. 9(1), pp 19-35

Krähenbühl R (2006) Der Felssturz, der sich auf die Stunde genau ankündigte. Bull. Angew. Geol. 11(1), pp 49-63

Krainer K, Mostler W, Span N (2002) A glacierderived, ice-cored rock glacier in the western Stubai Alps (Austria): evidence from ice exposures and Ground Penetrating Radar investigation. Zs. f. Gletscherkunde u. Glazialgeologie, Innsbruck, 38(1), pp 21-34

Lang A, Moya J, Corominas J, Schrott L, Dikau R (1999) Classic and new dating methods for assessing the temporal occurrence of mass movements. Geomorphology 30, pp 33-52

Leobacher A, Liegler K (1998) Langzeitkontrolle von Massenbewegungen der Stauraumhänge des Speichers Durlaßboden. Felsbau 16(3), pp 184-193

Lomax A, Virieux J, Volant P, Berge C (2000) Probabilistic earthquake location in 3D and layered models: Introduction of a Metropolis-Gibbs method and comparison with linear locations. In: Thurber CH, Rabinowitz N (ed) Advances in Seismic Event Location, Kluwer, Amsterdam, pp 101-134

Magotra N, Ahme N, Chael E (1987) Seismic event detection and source location using single-station (three-component) data. Bulletin of the Seismological Society of America, 77(3), pp 958-971

Marchesoni V (1958) La datazione col metodo del carbonio 14 del Lago di Molveno e dei resti vegetali riemersi in seguito allo svaso. Studi trentini d scienze naturali, Trento, (cit. in: Abele 1974), pp 95-98

Mertl S, Brückl E (2007) Detection and localization of micro-earthquakes on deep-seated mass movements. Geophysical Research Abstracts, Vol. 9, 07187

Noverraz FI (1996) Sagging or deep-seated creep: Fiction or reality? In. Senneset (ed) Proceedings of the 7th International Symposium on Landslides, Balkema, Rotterdam, pp 821-828

Ostermann M, Sanders D, Prager C, Kramers J (2007) Aragonite and calcite cement "boulder-controlled" meteoric environments on the Fern Pass rockslide (Austria): implications for radiometric age-dating of catastrophic mass movements, Facies 53, pp 189-208

Patzelt G (1977) Der zeitliche Ablauf und das Ausmass postglazialer Klimaschwankungen in den Alpen. In: Frenzel B (ed) Dendrochronologie und postglaziale Klimaschwankungen in Europa, Steiner, Wiesbaden, pp 248-259

Patzelt G (1987) Untersuchungen zur nacheiszeitlichen Schwemmkegel- und Talentwicklung in Tirol. Veröff. Mus. Ferdinandeum, Innsbruck 67, pp 93-123

Patzelt G, Poscher G (1993) Der Tschirgant-Bergsturz. Arbeitstagung 1993 Geol. B.-A., Geologie des Oberinntaler Raumes, Schwerpunkt Blatt 144 Landeck, Exkursion D: Bemerkenswerte Geologische und Quartärgeologische Punkte im Oberinntal und aus dem äußerem Ötztal, pp 206-213

Patzelt, G., 2004: Tschirgant-Haiming-Pletzachkogel. Datierte Bergsturzereignisse im Inntal und ihre talgeschichtlichen Folgen. Öffentl. Vortrag, 13.10.2004, alpS Symposium Naturgefahren Management 2004, Galtür

Podvin P, Lecomte I (1991) Finite difference computation of traveltimes in very contrasted velocity models: a massively parallel approach and its associated tools. Geophys. J. Int. 105, pp 271-284

Poscher G, Patzelt G (2000) Sink-hole Collapses in Soft Rocks. Felsbau, Rock and Soil Engineering 18(1), pp 36-40

Prager C, Krainer K, Seidl V, Chwatal W (2006) Spatial features of Holocene Sturzstrom-deposits inferred from subsurface investigations (Fernpass rockslide, Tyrol, Austria). Geo.Alp 3, pp 147-166

Prager C, Zangerl C, Brandner R & Patzelt G (2007) Increased rockslide activity in the Middle Holocene ? New evidences from the Tyrolean Alps (Austria). In: McInnes R, Jakeways J, Fairbank H & Mathie E (eds), Landslides and Climate Change, Challenges and Solutions, Taylor & Francis, pp 25-34

Prager C, Ivy-Ochs S, Ostermann M, Synal HA, Patzelt G (2008a) Geology and radiometric 14C-, 36Cl- and Th-/U-dating of the Fernpass rockslide (Tyrol, Austria), Geomorphology, in press

Prager C, Zangerl C, Patzelt G, Brandner R. (2008b) Age distribution of fossil landslides in the Tyrol (Austria) and surrounding areas. Nat. Hazards Earth Syst. Sci., in press

Raetzo-Brülhart H (1997) Massenbewegungen im Gurnigelflysch und Einfluss der Klimaänderung. Arb.-Ber. NFP 31, Hochsch.-Verlag. ETH Zürich

Renk D (2006) Geotechnische Untersuchungen von Gleitzonenmaterialien großer Hangbewegungen. Master thesis, Universität Karlsruhe (TH), Universität Innsbruck

Rott H, Scheuchl B, Siegel A, Grasemann B (1999) Monitoring very slow slope movements by means of SAR interferometry: A case study from a mass waste above a reservoir in the Ötztal Alps, Austria. Geophysical Res. Letters 26(11), pp 1629-1632

Ruina A (1983) Slip instability and state variable friction laws. Journal of Geophysical Research 88, pp 10359-10370

Sarnthein v.R (1940) Moor- und Seeablagerungen aus den Tiroler Alpen und ihre waldgeschichtliche Bedeutung. II. Teil: Seen der Nordtiroler Kalkalpen. Beih. Botan. Zentralblatt, LX, Abt. B (3), pp 437-492

Sartori M, Baillifard F, Jaboyedoff M, Rouille JD (2003) Kinematics of the 1991 Randa rockslides (Valais, Switzerland). Natural Hazards and Earth System Sciences 3, pp 423-433

Sass O, Wollny K (2001) Investigations regarding alpine talus slopes using ground-penetrating radar (GPR) in the Bavarian Alps, Germany. Earth Surf. Process. Landforms 26, pp 1071-1086

Scheikl M, Angerer H, Dölzlmüller J, Poisel R, Poscher G (2000) Multidisclinary Monitoring Demonstrated in the Case Study of the Eiblschrofen Rock fall. Felsbau 18(1), pp 24-29

Schmidegg O (1966) Bericht Staudamm Gepatsch, Geologie im Speicherbecken. Unveröffentlichter Bericht, K13-392, TIWAG Innsbruck

Schneider-Muntau B, Renk D, Marcher T, Fellin W (2006) The Importance of Laboratory Experiments in Landslide Investigation. In: Nadim F, Pöttler R, Einstein H, Klapperich H, Kramer S (ed) Geohazards, ECI Symposium Series, Volume P7 (2006). http://services.bepress.com/eci/geohazards/12

Soldati M, Corsini A, Pasuto A (2004) Landslides and climate change in the Italian Dolomites since the Late glacial. Catena 55, pp 141-161

Tentschert E (1998) Das Langzeitverhalten der Sackungshänge im Speicher Gepatsch (Tirol, Österreich). Felsbau 16(3), pp 194-200

Varnes DJ (1978) Slope Movement Types and Processes. In: Schuster RL, Krizek RJ (ed) Landslides-Analysis and Control, Special Report 176 (2), Washington D.C. (National Academy of Sciences), pp 11-33

Voight B (1988) Material science law applies to time forecasts of slope failure. In: Bonnard C. (ed), Landslides, Proceedings of the 5th International Symposium on Landslides, Lausanne, Switzerland, Balkema, Vol 3, pp 1471-1472

Wagner GS, Owens TJ (1996) Signal detection using multi-channel seismic data. Bulletin of the Seismological Society of America, 86(1A), pp 221-231

Watkins JS, Walters LA, Godso LA (1972) Dependence of in-situ compressional wave velocity on porosity in unsaturated rocks, Geophysics 37(1), pp 29-35

Watson AD, Martin CD, Moore DP, Stewart, TWG, Lorig LJ (2006) Integration of Geology, Monitoring and Modelling to Assess Rockslide Risk. Felsbau 24(3), pp 50-58

Weidner S (2000) Kinematik und Mechanismus tiefgreifender alpiner Hangdeformationen unter besonderer Berücksichtigung der hydrogeologischen Verhältnisse. Dissertation, Friedrich-Alexander Universität Erlangen-Nürnberg

Willenberg H (2004) Geologic and kinematic model of a complex landslide in crystalline rock (Randa, Switzerland). Dissertation Thesis, ETH Zurich, No. 15581, p 184

Yilmaz O (1987) Seismic Data Processing, Seismic data processing: Soc. of Expl. Geophys, p 526

Zangerl C, Eberhardt E, Schönlaub H, Anegg J (2007) Deformation behaviour of deep-seated rockslides in crystalline rock. In: Proceeding of the 1st Canada - U.S. Rock Mechanics Symposium, Vancouver, Canada, pp 901-908

Zischinsky U (1969) Über Sackungen. Rock Mechanics, 1, pp 30-52